INFLUENCE OF SURFACE ROUGHNESS ON AXIAL ACOUSTIC ENERGY DISTRIBUTION IN A PARABOLIC REFLECTOR

Zoran Milivojević
Engineering Academy of Serbia, Department of Electrical and Computer Engineering, Belgrade, Serbia, zoran.milivojevic@akademijanis.edu.rs
Violeta Stojanović
Academy of Technical and Educational Studies, Niš, Serbia, violeta.stojanovic@akademijanis.edu.rs
Dijana Kostić
Šargan Inženjering, Niš, Serbia, dijanaaricija79@gmail.com

Abstract: This paper analyzes the effect of surface roughness of an acoustic parabolic reflector on the scattering of acoustic energy outside the focal region. First, a formulation for calculating the gain of a parabolic reflector is presented as a function of its geometrical parameters, including the reflector depth H, aperture radius R, and focal position z_F. The gain is then evaluated as a function of the acoustic wavelength λ for reflectors constructed in the courtyard of the Academy of Technical and Educational Applied Studies in Niš, Serbia. The reflecting surface of the reflector is not smooth but rough, which leads to a degradation of acoustic energy concentration E at the focus, i.e., to increased scattering of acoustic energy along the axial z-direction. In the second part of the paper, an experiment is described in which the spatial distribution of acoustic energy $E(z_i)$ is determined from measurements of acoustic impulse responses along the z-axis. Subsequently, by applying statistical parameters (the energy centroid z_{eff}, standard deviation σ, position of the maximum z_{max}, full width at half maximum (FWHM), focusing efficiency η, and entropy H) the influence of surface roughness on the scattering of acoustic energy outside the focal region is quantified.
Keywords: Acoustics, parabolic reflectors, gain, impulse response, polar characteristics.

1. INTRODUCTION

The ability of curved reflecting surfaces to concentrate sound has been known for a long time (Coile, 1939). These principles were applied in the construction of early amphitheaters, churches, and similar structures. Paraboloids and ellipsoids are obtained by rotating a parabola and an ellipse about their axis of symmetry, producing surfaces with a focal point. Under appropriate excitation conditions (i.e., when the incident wavefront is normal to the reflector aperture), such surfaces can concentrate acoustic waves, i.e., acoustic energy. Paraboloidal surfaces are referred to as paraboloidal acoustic reflectors. However, in engineering practice, the term parabolic reflector is commonly used, despite the fact that the structure is inherently three-dimensional. The use of parabolic wall surfaces in churches to improve acoustic performance was analyzed in detail in (Cremer, 1948). During World War I and World War II, parabolic reflectors were employed for military purposes, primarily for the detection of enemy aircraft (e.g., zeppelins and airplanes) (Hefler, 2009). In addition to their application in concentrating acoustic waves, parabolic reflectors are also widely used for focusing electromagnetic waves, such as light and radio waves (e.g., satellite and radar antennas) (Yi & Haberman, 2013). In (Olson & Wolff, 1930), a directional microphone based on a parabolic reflector with a microphone positioned at the focus is presented. The authors report that such a configuration behaves as a horn at low frequencies and as a reflector at high frequencies. The application of a parabolic reflector for estimating the direction of arrival of an acoustic wave is described in (Saka & Kaderli., 1998). The geometry of a parabola ensures that, under ideal conditions, a plane wave incident along the axis is focused at a single point, referred to as the focus, assuming specular reflection from a smooth surface (Cabrera et al., 2023; Zhang et al., 2020). Consequently, a parabolic reflector is often treated as an acoustic amplifier. The acoustic characteristics of parabolic reflectors have been studied extensively over many years (Olson & Wolff, 1930; Little, 1966; Chen et al., 2019; Chen et al., 2018). In (Wahlstrom, 1985), an analytical expression for the reflector gain is derived as a function of its geometry (the aperture radius, reflector depth, and focal length) as well as the frequency of the acoustic wave. In recent years, research has extended beyond classical parabolic geometries toward advanced reflective structures, including acoustic retroreflectors, metasurfaces, and architecturally integrated focusing systems, which demonstrate enhanced control of sound reflection and energy concentration (Cabrera et al., 2023; Rapp et al., 2022; Zhu et al., 2021).

In (Milivojević, 2018), the characteristic geometries of acoustic reflectors are presented as functions of reflector depth, aperture diameter, and focal position. Furthermore, based on the results reported in (Wahlstrom, 1985), the dependence of the gain of an acoustic parabolic reflector on its geometrical parameters is analyzed as a function of acoustic wave frequency. In the gain calculation, it is assumed that the reflecting surface is ideally smooth and that the reflection coefficient is equal to unity, i.e., no energy absorption occurs at the reflecting surface and perfect specular reflection is achieved. The same study (Milivojević, 2018) provides the theoretical gain of acoustic parabolic reflectors constructed, according to the design of the first author, in the courtyard of the Academy of Technical and Educational Applied Studies in Niš. In (Stojanović & Milivojević, 2024), an experiment is described in which the acoustic impulse responses and polar characteristics of these reflectors are determined.

However, in the practical implementation of the acoustic reflectors, a construction-related deviation was introduced. Specifically, the reflecting surface was intentionally made rough, most likely to match the texture of the surrounding environment (the courtyard of the Academy), resulting in a pronounced surface relief. This modification led to changes in the acoustic performance of the reflector. The effect of surface roughness manifests as increased scattering of acoustic energy outside the focal region and, consequently, a reduction in focusing efficiency.

In this paper, the scattering of acoustic energy is evaluated. An experiment was conducted in which acoustic impulse responses were measured along the *z*-axis (axis of symmetry) at a set of measurement points (MPs). Based on these measurements, the acoustic energy E of the wave emitted from the second reflector was determined. Subsequently, the scattering of acoustic energy was quantified using statistical parameters, including the standard deviation σ, full width at half maximum (FWHM), system efficiency η, and entropy H. The experimental results are presented in both tabular and graphical form. The analysis indicates a degradation in reflector performance compared to the ideal case (i.e., a perfectly smooth reflecting surface), thereby confirming the significant influence of the reflecting surface microgeometry on the overall system behavior.

The remainder of the paper is organized as follows. Section II presents the formulas used to calculate the gain of the acoustic parabolic reflector. Section III describes the dimensions of the constructed reflector and provides the calculated gain and polar characteristics. Section IV describes the experiment conducted to evaluate the scattering of acoustic energy. Section V concludes the paper.

2. IDEAL PARABOLIC REFLECTOR

The geometry of a parabolic reflector in the (r,z) plane is described by the parabola:

$$r^2 = 4 \cdot z_F \cdot z \,, \qquad (1)$$

where z_F denotes the focal position. By rotating the parabola about the z-axis, a paraboloid is obtained. By limiting the paraboloid to the interval $z \in [0,H]$, a truncated paraboloid representing the acoustic parabolic reflector is obtained. The reflector depth is denoted by H, while R is the aperture radius. The vertex of the reflector is located at (0,0). A plane wavefront parallel to the z-axis, upon entering the reflector aperture, is focused at the focal point z_F. In [11], a procedure for deriving the analytical expression for the theoretical gain of the reflector is presented. The resulting expression can be written in the form:

$$F_z = \sqrt{1+\left[4\pi\, z_F/\lambda \cdot \ln\left(1+H/z_F\right)\right]^2 + 8\pi z_F/\lambda \cdot \ln\left(1+H/z_F\right)\sin\left(4\pi z_F/\lambda\right)} = \left|1 + A \cdot e^{iB}\right| \,, \qquad (2)$$

where $A = 4\pi \cdot z_F/\lambda \cdot \ln\left(1+H/z_F\right)$ and $B = 4\pi \cdot z_F/\lambda$. In (2), the following terms are defined: (a) '1' represents the normalized direct wave; (b) $A^2 = \left[4\pi \cdot z_F/\lambda \cdot \ln\left(1+H/z_F\right)\right]^2$ represents the energy of the reflected wave; (c) the ratio z_F/λ describes the reflector size to the wavelength λ; (d) $\ln\left(1+H/z_F\right)$ accounts for the reflector geometry; (e) $2 \cdot A \cdot \sin\left(B\right)$ represents the interference between the direct and reflected waves; (f) $B = 4\pi \cdot z_F/\lambda$ denotes the phase difference between the direct and reflected waves. When $\lambda = 8 \cdot z_F \Rightarrow \sin\left(4\pi\, z_F/\lambda\right) = \pm 1$, it follows that condition, yielding $F_z = 4\pi\, z_F/\lambda \cdot \ln\left(1+H/z_F\right)$. For high gain values (i.e., when the reflector dimensions are large compared to the wavelength), $H = R^2/(4 \cdot z_F)$, and therefore $F_z = 4\pi \cdot z_F/\lambda \cdot \ln\left(1+R^2/4z_F^2\right)$. When $R^2/(4 \cdot z_F) >> 1$, it follows that $\ln\left(1+R^2/4z_F^2\right) \approx \ln\left(R^2/4z_F^2\right)$, and thus the final expression for the reflector gain becomes:

$$F_z \approx 4\pi \cdot z_F/\lambda \cdot \ln\left(R^2/4z_F^2\right) . \qquad (3)$$

The gain of a parabolic reflector depends on its geometrical parameters (h, R, z_F) and is a function of frequency, i.e., the acoustic wavelength λ. The gain expressed in decibels is given by:

$$G = 20 \cdot \log_{10}\left(F_Z\right) . \qquad (4)$$

3. PARABOLIC REFLECTOR - CONSTRUCTION

In the courtyard of the Academy of Technical and Educational Applied Studies in Niš, a system of acoustically coupled, mutually identical parabolic reflectors (Refl. 1 and Refl. 2) was constructed according to the design of the first author (Fig. 1.a). The dimensions of the acoustic reflectors are as follows: (a) depth H = 0.3571 m, (b) aperture radius R = 1 m, and (c) focal length z_F = 0.7 m. The distance between the reflector vertices is l = 23 m (Fig. 1.b). The reflectors are made of reinforced concrete. Given that H/z_F = 0.3571 / 0.7 = 0.51 the reflector gain $G(z_F/\lambda)$ [dB] was calculated as a function of frequency f, i.e., wavelength λ, using (4). The gain $G(z_F/\lambda)$ in logarithmic scale is shown in Fig. 2.a (Stojanović & Milivojević, 2024). By measuring acoustic impulse responses for angles θ = -90°:15°: 90°, the polar characteristic $E(\theta)$ was obtained and presented in normalized form $E(\theta)/E(0°)$ in the polar diagram shown in Fig. 2.b (Stojanović & Milivojević, 2024).

Fig. 1. Acoustic parabolic reflectors: (a) system of coupled acoustic reflectors (Refl. 1 and Refl. 2); (b) view of parabolic reflector 1 (Refl. 1); and (c) detail of the surface roughness of the reflecting surface of Refl. 1.

a) b) c)

Source: Authors' own photographs, taken on April 27, 2026, at the Academy of Technical and Educational Vocational Studies, Niš, Serbia.

Fig. 2. (a) Theoretical gain of the acoustic parabolic reflector $G(z_F/\lambda)$; (b) normalized polar characteristic $E(\theta)/E(0°)$.

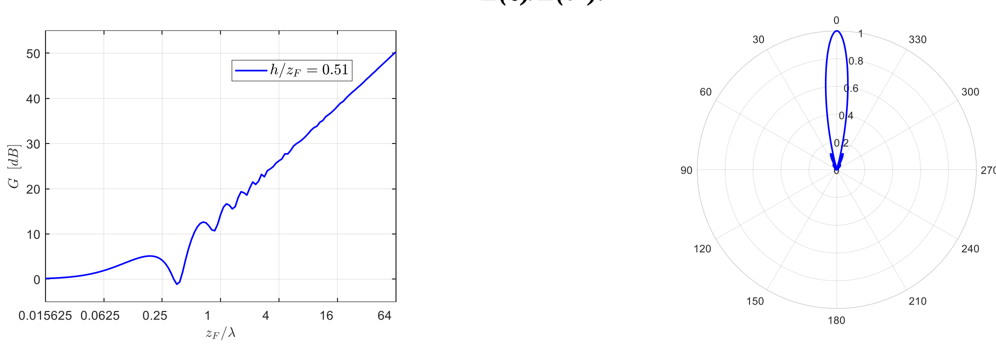

a) b)

Source: Diagrams reproduced from the paper by Stojanović and Milivojević (2024).

4. MEASUREMENT OF SCATTERING DUE TO SURFACE ROUGHNESS

During construction, the contractor introduced a modification without consultation with the project author. Most likely for aesthetic reasons, and in order to match the texture of the surrounding courtyard, the reflecting surface was made rough instead of ideally smooth. As a result, an acoustic wave incident normally and propagating parallel to the z-axis, upon entering the reflector aperture, deviates from ideal specular reflection and is no longer focused at the focal point, but instead is scattered in its vicinity. This leads to diffuse scattering and a loss of phase coherence. The scattering of acoustic energy was determined experimentally and is presented using a set of statistical parameters.

4.1. Experiment

The experiment was conducted with the aim of measuring the spatial distribution of acoustic energy of Refl. 1 along the axis of symmetry (the z-axis), and, based on these results, determining statistical parameters that describe the scattering of energy around the focal point z_F. The experiment was carried out in the following steps: *Step 1*: At measurement points MP_i, i = 1, ..., N, acoustic impulse responses h_i were recorded, with the acoustic excitation emitted from the focus of Refl. 2. *Step 2*: The acoustic energy E_i at MP_i was calculated for a test signal x_T emitted

from the focus of Refl. 2. *Step 3*: Statistical parameters describing the energy distribution along the z-axis and its scattering around the focal point z_F were computed.
Step 1 was carried out using an experimental setup consisting of an omnidirectional microphone (PCB 130D20), a B&K omnidirectional sound source (Type 4295), a B&K audio power amplifier (100 W RMS, Type 2716-C), and a laptop equipped with a SoundMax Integrated Digital Audio sound card. The recordings were performed using the EASERA software package. The excitation signal was a sine sweep of duration t = 5 s. The measurement points MP_i, $i = 1,\ldots,N$ with N_{MP} =23, were located along the z-axis at positions z_i = [35 40 45 50 55 60 65 70 75 80 85 95 100 105 110 120 130 140 150 170 180 190 200] cm. The sine sweep acoustic signal was emitted from the focus of Refl. 2. In *Step 2*, the test signal is defined as $x_T = \sin(2\pi f t)$. The acoustic energy E_i was computed by convolving the measured impulse response h_i with the test signal x_T, followed by squaring the result, using MATLAB software ($E_i = \mathrm{conv}(h_i, x_T)^2$). In *Step 3*, for the measurement points z_i and the corresponding acoustic energy values E_i, statistical parameters were computed in discrete form, taking into account non-uniform sampling through weighting factors Δz_i. (a) The total energy along the z-axis is $E_{\text{total}} \approx \sum_{i=1}^{N} E_i \cdot \Delta z_i$, (b) The effective focal position, defined as the centroid of the energy distribution, is $z_{\text{eff}} \approx \sum_{i=1}^{N} z_i E_i \Delta z_i \Big/ \sum_{i=1}^{N} E_i \Delta z_i$, (c) The standard deviation, describing the spread of energy around the effective focal position $\sigma \approx \left(\sum_{i=1}^{N} (z_i - z_{\text{eff}})^2 E_i \Delta z_i \,/\, \sum_{i=1}^{N} E_i \Delta z_i \right)^{1/2}$, (d) The maximum value of the distribution and the corresponding position are defined as $E_{\max} = \max_{z} E(z)$, $z_{\max} = z_{i^*}$, $i^* = \arg\max_{i} E_i$, (e) The full width at half maximum FWHM = z_2 - z_1, where z_1 and z_2 are the positions at which the distribution reaches half of its maximum value. (f) The focusing efficiency, defined as the fraction of energy concentrated in the vicinity of the focal region $\eta \approx \sum_{z_i \in [z_{\text{eff}} - \sigma, z_{\text{eff}} + \sigma]} E_i \Delta z_i \Big/ \sum_{i=1}^{N} E_i \Delta z_i$, (g) The Shannon entropy is defined as $H = -\sum_{i=1}^{N} p_i \log p_i$ where p_i represents the normalized energy distribution, satisfying $\sum_{i=1}^{N} p_i = 1$.

4.2. Experimental Results

Fig. 3 shows the impulse responses h and the corresponding amplitude characteristics in logarithmic scale for three characteristic measurement points: (a) Fig. 3.a, MP_1, closest to the reflector vertex (z_1 = 35 cm); (b) Fig. 3.b, MP_8, located at the focal point (z_8 = 70 cm); and (c) Fig. 3.c, MP_{23}, farthest from the vertex (z_{23} = 200 cm). The distribution of acoustic energy E at the measurement points along the z-axis (*Step 3*), following excitation by the test signal x_T, is shown in Fig. 4: (a) fig. 4.a (f = 63 Hz), (b) fig. 4.b (f = 125 Hz), (c) fig. 4.c (f = 250 Hz), (d) fig. 4.d (f = 500 Hz), (e) fig. 4.e (f = 1 kHz), (f) fig. 4.f (f = 2 kHz), (g) fig. 4.g (f = 4 kHz) and (h) fig. 4.h (f = 8 kHz). The statistical parameters of the energy distribution along the z-axis are presented in Table I and in Fig. 5: (a) Fig. 5.a (FWHM), (b) Fig. 5.b (σ), (c) Fig. 5.c (η), and (d) Fig. 5.d (z_{eff} and z_{max}).

Fig. 3. Acoustic impulse responses and amplitude characteristics in logarithmic scale at the measurement points: (a) MP_1 (z_1 = 35 cm), (b) MP_8 (z_8 = 70 cm) i (c) MP_{23} (z_{23} = 200 cm).

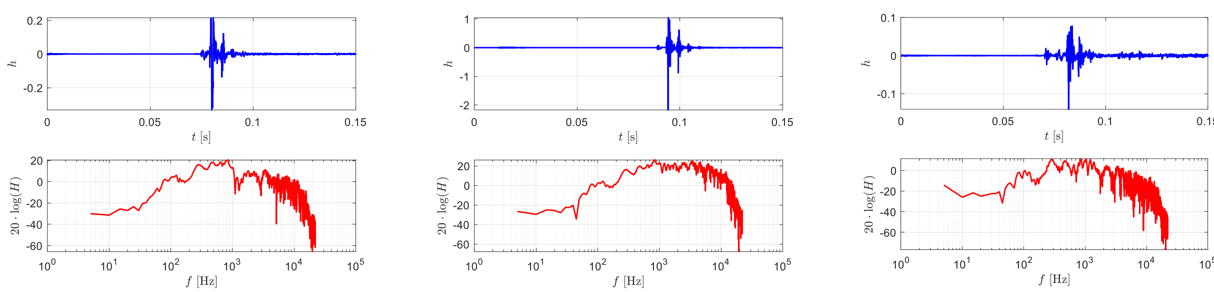

a) b) c)

Source: Result obtained in the Step 1 experiment conducted by the authors.

4.3. Results Analysis

Based on the results presented in Table I and Figs. 2–5, a pronounced dependence of the focusing characteristics on frequency can be observed. Accordingly, three frequency ranges can be identified and analyzed:
(a) In the low-frequency range (f < 500 Hz), effective focusing is not achieved, and a diffuse energy distribution dominates: (i) large distribution width (FWHM = 65–75 cm), (ii) significant deviation between the position of the

maximum and the effective focus zmax □ zeff, (iii) low efficiency (η ≈ 0.56–0.61), and (iv) high entropy (H ≈ 0.79). This behavior is a consequence of the wavelength being larger than the characteristic dimensions of the reflector, with diffraction effects dominating. (b) In the mid-frequency range (f ≈ 500 Hz), the onset of acoustic energy focusing toward the focal region is observed: (i) zmax = 70 cm, and (ii) the standard deviation σ begins to decrease. However, the FWHM remains at the same level as in the low-frequency range (FWHM = 75 cm), and the efficiency is still low (η = 0.6148), indicating that the focus is not yet fully formed and that a significant portion of the energy is not concentrated around the focal point. (c) In the high-frequency range (f ≥ 1 kHz), a focal region is formed: (i) with increasing frequency, the distribution width decreases (FWHM = 35–5 cm), (ii) the standard deviation decreases (σ = 28–12.6 cm), (iii) the efficiency increases (η > 0.7), and (iv) zmax □ 70 cm, zeff = 80.2-69.1 cm. A pronounced focusing effect with a symmetric focal region is observed. The standard deviation and entropy indicate the presence of residual energy scattering, which in this frequency range is primarily a consequence of the roughness of the reflecting surface.

Fig. 4. Energy distribution following excitation by the test signal x_T: (a) f = 63 Hz, (b) f = 125 Hz, (c) f = 250 Hz, (d) f = 500 Hz, (e) f = 1 kHz, (f) f = 2 kHz, (g) f = 4 kHz and (h) f = 8 kHz.

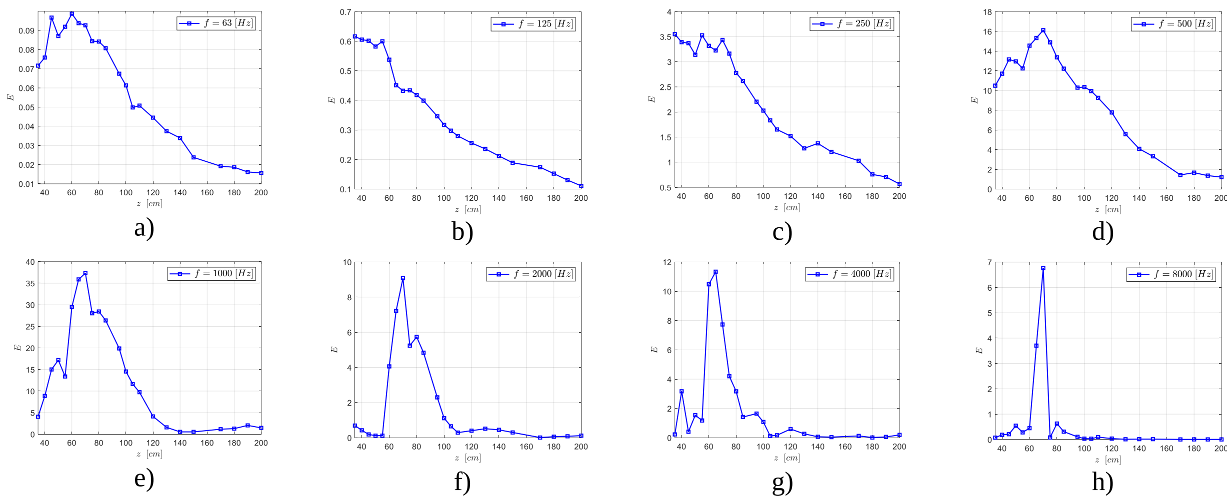

Source: Result obtained in the Step 2 experiment conducted by the authors.

Table I: Statistical parameters of the energy distribution along the z-axis

f [Hz]	z_{eff} [cm]	*σ* [cm]	FWHM [cm]	z_{max} [cm]	E_{max}	*η*	*H*	E_{tot}
63	91.7	40.7	75	60	0.0987	0.6105	0.7922	8.4817
125	94.6	44.7	65	35	0.6163	0.5891	0.7884	51.4791
250	93.7	43.2	70	35	3.5500	0.5625	0.7897	316.1525
500	88.3	36.3	75	70	16.1251	0.6148	0.7980	1269.7
1000	80.2	28.0	35	70	37.3277	0.7271	0.7910	1757.5
2000	80.7	22.4	20	70	9.0742	0.8199	0.7205	247.2995
4000	71.2	21.7	10	65	11.3347	0.7607	0.7424	259.9958
8000	69.1	12.6	5	70	6.7601	0.7990	0.6264	69.3465

Fig. 5. Statistical parameters of the acoustic energy distribution along the z-axis as a function of frequency: (a) FWHM, (b) σ, (c) η, and (d) z_{eff} and z_{max}.

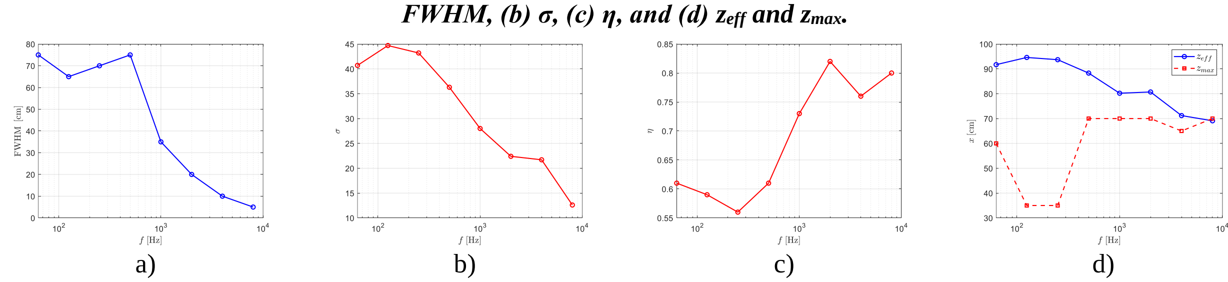

Source: Result obtained in the Step 3 experiment conducted by the authors.

In general, an increase in axial energy concentration with increasing acoustic frequency is observed, which is clearly demonstrated by the analysis of selected statistical parameters at the boundary frequencies f = 63 Hz and f = 8 kHz: (i) z_{eff}: 91.7 cm → 69.1 cm (ideal value: 70 cm), (ii) z_{max}: 60 cm → 70 cm, (iii) standard deviation σ: 40.7 cm → 12.6 cm, (iv) FWHM decreases: 75 cm → 5 cm, (v) efficiency η: 0.6105 → 0.799, and (vi) entropy H: 0.7922 → 0.6264. The focusing efficiency η increases with frequency and reaches saturation in the high-frequency range. This saturation indicates the presence of systematic losses that limit energy concentration at the focus and can be attributed to non-idealities of the reflecting surface, including its roughness. The entropy of the energy distribution H decreases with increasing frequency, indicating improved spatial localization and concentration of energy. However, the non-zero entropy values in the high-frequency range suggest the presence of significant energy components outside the focal region, which can be associated with surface roughness and diffuse scattering.

5. CONCLUSION

This paper analyzes the scattering of acoustic energy along the z-axis of an acoustic parabolic reflector using statistical parameters, including the effective focal position z_{eff}, standard deviation σ, full width at half maximum (FWHM), efficiency η, and entropy H. The experimental results clearly identify three frequency ranges: low-frequency ($f \leq 250$ Hz), mid-frequency ($f = 500$ Hz), and high-frequency ($f \geq 1$ kHz). In the low-frequency range ($f \leq 250$ Hz), very poor focusing performance is observed, characterized by high values of σ and H, low efficiency η, and unstable positions of the energy maximum. This behavior can be explained by the fact that the acoustic wavelength exceeds the characteristic dimensions of the reflector, leading to dominant diffraction effects. In this regime, the focal region is not formed, and z_{max} does not have a meaningful physical interpretation. In the mid-frequency range ($f = 500$ Hz), a significant reduction in FWHM and σ, accompanied by an increase in η, is observed, indicating the formation of a focal region and the transition toward a geometrically dominated regime. In the high-frequency range ($f \geq 1$ kHz), the decrease in FWHM, entropy H, and standard deviation σ, together with the increase in efficiency η, clearly indicates a transition from a diffraction-dominated to a focused regime, i.e., an increasing axial concentration of energy. The position of the energy maximum converges with increasing frequency such that $z_{eff} \approx z_{max} \approx 70$ cm, approaching the geometrical focal position $z_F = 70$ cm. However, the observed values of the standard deviation (σ = 28–12.6 cm) and entropy indicate the presence of residual energy scattering, which can be attributed, among other factors, to the roughness of the reflecting surface. With improved mechanical smoothing of the surface, a significant reduction in the standard deviation (to a few centimeters) is expected, leading to higher focusing efficiency ($\eta > 0.9$) and a corresponding decrease in the entropy parameter H. These results confirm the critical role of surface microgeometry in determining the focusing performance of acoustic parabolic reflectors and highlight the importance of surface quality in practical implementations.

REFERENCES

Cabrera, D., Lu, S., Holmes, J., & Yadav, M. (2023). The potential of focusing acoustic retroreflectors for architectural surface treatment. Applied Sciences, 13(3), 1547.

Cabrera, D., Lu, S., Holmes, J., Yadav, M., & Hutchison, O. (2023). Focusing acoustic retroreflectors for architectural applications. Applied Sciences, 13(3), 1547.

Chen, K., Irie, T, Iijima, T., & Morita, T. (2019). Double-parabolic-reflectors acoustic waveguides for high-power medical ultrasound. Scientific Reports, 9, 18493.

Chen, K., Irie, T., Iijima, T., & Morita, T. (2019). Acoustic focusing to the waveguides utilizing double parabolic reflectors. Applied Physics Letters, 114(7).

Coile, R. (1939). The parabolic sound concentrator, J. Acoust. Soc. Am. Vol. 11, 167.

Cremer, L. (1948). Die wissenschaftlichen Grundlagen der Raumakustik, Vol. 1, Geometrische Raumakustik, Zurich.

Hefler, M. (2009). Sound Source Localisation with Acoustic Mirrors, *NAG/DAGA*, pp. 1432-1453, Rotterdam.

Little, R. (1966). Acoustic properties of parabolic reflectors, J. Acoust. Soc. Am., Vol. 40, 919–920.

Milivojević, Z. (2018). Parabolični reflektor kao akustički pojačavač, *Zbornik radova Visoke tehničke škole strukovnih studija u Nišu*, 36 – 40.

Olson, H., & Wolff, I. (1930). Sound concentrator for microphones, J. Acoust. Soc. Am., Vol. 1, 410 - 417.

Rapp, M., Cabrera, D., & Lu, S. (2022). A polytrihedral dome for acoustic retroreflection and its applications. Applied Acoustics, 195, 108860.

Saka, B., & Kaderli, A. (1998). Direction of arrival estimation and adaptive nulling in array-fed reflectors, *MELECON '98, 9th Mediterranean Electrotechnical Conference*, 274 - 277, Tel-Aviv, Israel.

Stojanović, V., Milivojević, Z. (2024). The polar characteristic of an acoustic parabolic reflector, Facta Universitatis, Series: Working and Living Environmental Protection, 21(4), Special Issue, 293 – 303.

Wahlstrom, S. (1985) The parabolic reflector as an acoustical amplifier, J. Audio Eng. Soc., Vol. 33, 418–429.

Yi, T. Jinying, Z., & Haberman, M. (2013). Transient axial solution for plane and axisymmetric waves focused by a paraboloidal reflector, J. Acoust. Soc. Am. 133(4), 2025 - 2035.

Zhang, T., Geng, Y., Sun, J., & Chen Jiao, C. (2020). A unified speech enhancement system based on neural beamforming with parabolic reflector. Applied Sciences, 10(7), 2218.

Zhu, Y., Cao, L., Merkel, A., Fan, S.-W., Vincent, B., & Assouar, B. (2021). Janus acoustic metascreen with nonreciprocal and reconfigurable phase modulations. Nature Communications, 12, 7089.